

# Spontaneous Raman scattering in SDM fibers

LUCAS ALVES ZISCHLER<sup>1,\*</sup>, GIAMMARCO DI SCIULLO<sup>1</sup>, DIVYA A. SHAJI<sup>1</sup>, ANTONIO MECOZZI<sup>1</sup>, AND CRISTIAN ANTONELLI<sup>1</sup>

<sup>1</sup>Department of Physical and Chemical Sciences, University of L'Aquila, 67100 L'Aquila, Italy

\*lucas.zischler@univaq.it

Compiled February 23, 2026

**Spontaneous Raman scattering (SpRS) is a weak non-linear effect, particularly relevant to classical-quantum coexistence transmission and sensing applications. In classical transmission, the relevant Raman effect is stimulated Raman scattering (SRS), and recent studies have examined it in space-division multiplexing (SDM) fibers. An intrinsic relation between SpRS and SRS allows previous SRS results to inform SpRS models. In this work, we extend SpRS models derived for single-mode fibers (SMFs) to SDM fibers with multiple mode groups of degenerate modes, covering both Stokes and anti-Stokes bands. The proposed model is a useful, fiber-design-independent tool for evaluating scattered noise in optical links, and it is validated through experimental measurements in field-deployed multi-core fibers (MCFs) and multi-mode fiber (MMF), showing good agreement.**

<http://dx.doi.org/10.1364/ao.XX.XXXXXX>

In recent years, space-division multiplexing (SDM) has emerged as one of the leading technologies to sustain increasing traffic demands [1], and the additional spatial dimension has been exploited to benefit quantum key distribution (QKD) transmission [2]. Nevertheless, there is a lack of studies on spontaneous Raman scattering (SpRS) in SDM fibers, a phenomenon particularly crucial in classical-quantum coexistence scenarios [3].

In classical transmission, the relevant Raman effect is stimulated Raman scattering (SRS), and recent work have evaluated it in multi-core fibers (MCFs) [4] and multi-mode fibers (MMFs) [5–7]. Since both SRS and SpRS arise from the delayed Kerr response of silica, a simple relation linking the two efficiencies can be expected. This work provides analytical formulas linking SpRS noise power to Raman gain efficiency. We extend previously established SpRS models developed for the Stokes region in single-mode fibers (SMFs) [8, 9] to SDM fibers, including the anti-Stokes region. The proposed model addresses the most general case of SDM fibers featuring multiple groups of degenerate modes. The model is experimentally validated with measurements performed in a 4-core uncoupled-core multi-core fiber (UC-MCF), 4-core coupled-core multi-core fiber (CC-MCF), and a 15-mode graded-index MMF field-deployed in the city of L'Aquila, Italy [10]. Results show good agreement between theory and measurements.

Raman scattering can be described in quantum physics as a process where a pumped optical phonon decays to a lower energy state, with the Stokes shift determined by molecular vibrational losses. In classical wave theory, it corresponds to the delayed third-order non-linear susceptibility of the medium.

In the scalar case, neglecting losses of the fiber medium, the mean rate of scattered photons  $N_s$  in an infinitesimal segment  $dz$ , guided along the fiber with energy  $hf_s$  (where  $h$  is Planck's constant and  $f_s$  the photon frequency), is given by [Eq. (6) 9], [Eq. (11) 8], [Eq. (21) 11].

$$\pm \frac{dN_s(z)}{dz} = \begin{cases} [1 + \Phi(\Delta f)]g_R(f_p, \Delta f)P_p(z), & f_s < f_p, \\ \Phi(\Delta f)g_R(f_p, \Delta f)P_p(z), & f_s > f_p, \end{cases} \quad (1)$$

where,  $\pm$  accounts for the propagation direction,  $f_p$  is the pump frequency, and  $\Phi(\Delta f)$  is the thermally populated phonon occupancy factor, discussed in more detail below, with  $\Delta f = |f_s - f_p|$ . The coefficient  $g_R$  represents the SRS efficiency, and  $P_p(z)$  denotes the optical power at the pump frequency  $f_p$  and distance  $z$ . The SRS coefficient accounts only for the portion of the Raman cross-section resulting in guided photons. The photon rate can be expressed in power units as  $P_s^{\text{SpRS}}(z) = hf_s B_{\text{ref}} N_s(z)$ , where  $B_{\text{ref}}$  is a reference bandwidth. In contrast to SRS, SpRS produces scattered photons in both propagation directions.

In the Stokes region, the factor  $[1 + \Phi(\Delta f)]$  accounts for phonons in the ground vibrational state plus thermally populated phonons with vibrational energy  $h\Delta f$ , which follow Bose-Einstein statistics  $\Phi(\Delta f) = \{\exp[h\Delta f / (k_B T)] - 1\}^{-1}$ .

In the anti-Stokes process, only phonons in a higher vibrational state produce scattered light, when decaying to lower energy states. Albeit weaker, anti-Stokes SpRS is always present in real setups, as thermally loaded phonons can provide the energy needed to produce photons with a positive frequency shift.

When multiple spatial modes and polarizations are present, the Raman effect can encompass all distinct spatial paths. The SRS efficiency from the  $h^{\text{th}}$  to the  $i^{\text{th}}$  mode is given by [12]

$$g_{R,ih}(f_p, \Delta f) = \frac{\pi}{4} f_s \chi^{(3)} \epsilon_0 h_R(\Delta f) A_{\text{eff},ih}^{-1}(f_p, f_s), \quad (2)$$

where  $\chi^{(3)}$  is the third-order susceptibility coefficient,  $h_R(\Delta f)$  is the material's Raman parallel-polarized impulse response<sup>1</sup> [Eq. (6) 13], and  $\epsilon_0$  is the vacuum permittivity. We

<sup>1</sup>The cross-polarized response is neglected due to its negligible magnitude in silica fibers.

approximate the fiber as a homogeneous medium, so the Raman impulse response is independent of the mode profile, where this assumption is later validated with experimental measurements. The self- or cross-effective mode area  $A_{\text{eff},i,h}(f_p, f_s)$  is given by [Eq. (7) 14]

$$A_{\text{eff},i,h}(f_s, f_p) = \frac{\iint \|\vec{F}_i(x, y, f_s)\|^2 dx dy \iint \|\vec{F}_h(x, y, f_p)\|^2 dx dy}{\iint \|\vec{F}_i(x, y, f_s) \cdot \vec{F}_h(x, y, f_p)\|^2 dx dy}, \quad (3)$$

where  $\vec{F}_i(x, y, f)$  is the  $i^{\text{th}}$  mode profile at frequency  $f$ .

It is therefore convenient to define a mode-independent Raman response that can be extracted from the SRS efficiency, defined as

$$\hat{g}_R(f_p, \Delta f) = \frac{\pi}{4} f_s \chi^{(3)} \epsilon_0 h_R(f_p, f_s). \quad (4)$$

The modes can be grouped into weakly-coupled groups of degenerate modes. The SRS gain efficiency, averaged over the mode groups, scales by the inverse of the self- and cross-mode-group-averaged effective areas, given by

$$\tilde{A}_{\text{eff},n,m}(f_s, f_p) = \frac{4N_n(f_s)N_m(f_p)}{\sum_{\substack{i \in [1, 2, \dots, N_n(f_s)] \\ h \in [1, 2, \dots, N_m(f_p)]}} A_{\text{eff},i,h}^{-1}(f_p, f_s)}, \quad (5)$$

where  $N_n(f)$  is the number of spatial modes in the  $n^{\text{th}}$  mode group at frequency  $f$ . The indices  $i$  and  $h$  span all spatial modes and polarizations. The mode-group-averaged SRS efficiency is then given by  $\tilde{g}_{R,n,m}(f_p, \Delta f) = \hat{g}_R(f_p, \Delta f) \tilde{A}_{\text{eff},n,m}^{-1}(f_s, f_p)$ .

Under the assumption that all modes within a given mode group  $n$  are statistically equivalent, the mode-group-averaged SpRS power satisfies the following evolution equation

$$\pm \frac{dP_{s,n}^{\text{SpRS}}(z)}{dz} = -\alpha_n(f_s) P_{s,n}^{\text{SpRS}}(z) + \sum_{m \neq n} \kappa_{n,m}(f_s) P_{s,m}^{\text{SpRS}}(z) + \sum_m \eta_{n,m}(f_p, \Delta f) P_{p,m}^{\text{T}}(z), \quad (6)$$

where  $\alpha_n(f)$  is the mode-group-averaged attenuation profile,  $\kappa_{n,m}(f)$  the coupling coefficient between mode groups  $n$  and  $m$ , and  $P_{p,m}^{\text{T}}(z)$  is the total power in mode group  $m$  at frequency  $f_p$  and distance  $z$ . The coefficient  $\eta_{n,m}(f_p, \Delta f)$  represents the SpRS efficiency from the  $m^{\text{th}}$  to the  $n^{\text{th}}$  mode group, given by

$$\eta_{n,m}(f_p, \Delta f) = \begin{cases} [1 + \Phi(\Delta f)] h f_s B_{\text{ref}} \tilde{g}_{R,n,m}(f_p, \Delta f), & f_s < f_p, \\ \Phi(\Delta f) h f_s B_{\text{ref}} \tilde{g}_{R,n,m}(f_p, \Delta f), & f_s > f_p. \end{cases} \quad (7)$$

Similarly to the SRS efficiency, a SpRS coefficient  $\hat{\eta}(f_p, \Delta f)$  solely dependent on the material characteristics can be defined as

$$\eta_{n,m}(f_p, \Delta f) = \hat{\eta}(f_p, \Delta f) \tilde{A}_{\text{eff},n,m}^{-1}(f_s, f_p). \quad (8)$$

We utilized the proposed model to characterize the SpRS efficiency on two types of MCFs, UC-MCF and CC-MCF, both with 4 cores and equal single-core self-effective mode area ( $81 \mu\text{m}^2$  at  $1550 \text{ nm}$  [15],  $162 \mu\text{m}^2$  polarization-mode averaged cross-effective area). The cores of the UC-MCF are single-mode and experience minimal inter-core coupling. In the CC-MCF, the cores are strongly coupled and the local modes form a single group of degenerate modes.

All experimental measurements were performed with a Raman pump at  $1455 \text{ nm}$ . The SRS measurements were performed in [4], and are briefly reviewed here. The SRS efficiency was estimated from the on-off Raman gain of a probe signal, which

was swept from  $1500 \text{ nm}$  to  $1620 \text{ nm}$ . The probe was co- and counter-propagated relative to the pump in the CC-MCF. The signal power was measured with an optical spectral analyzer (OSA) both with the pump on and off. To remove the SpRS contribution from the on-off Raman gain measurements, an additional measurement was performed with the pump on and the signal off. At the fiber input, the pump was attached to a single core in both fiber types. The optical power was measured in the core under test in the UC-MCF, and simultaneously measured from all fiber cores with a power coupler in the CC-MCF case.

In the UC-MCF measurements, the pump was launched in a  $25.3\text{-km}$  long fiber link with measured optical power of  $17.95 \text{ dBm}$ . For the CC-MCF measurements, the pump was launched in a  $69.3\text{-km}$  long link with measured optical power of  $29 \text{ dBm}$ . In both scenarios, the probe signal was launched with a measured optical power of  $-35 \text{ dBm}$  per core.

The results for the mode-group-averaged SRS efficiency are shown in Fig. 1(a). In the CC-MCF, the optical power is distributed over an effective cross-section area four times larger, reducing the group-averaged SRS coefficient by a factor of four.

For the CC-MCF and for each core of the UC-MCF Eq. (6) reduces to differential equations of the same form. Solving the reduced equation for  $P_{s,n}^{\text{SpRS}}(z)$  yields an analytical relation between group-averaged SpRS efficiency and fiber parameters, given as

$$\eta(f_p, \Delta f) = \begin{cases} \frac{P_s^{\text{SpRS}}(L) \exp[\alpha(f_s)L]}{\int_0^L P_p^{\text{T}}(z') \exp[\alpha(f_s)z'] dz'} & \text{Co-prop.}, \\ \frac{P_s^{\text{SpRS}}(0)}{\int_0^L P_p^{\text{T}}(z') \exp[-\alpha(f_s)z'] dz'} & \text{Counter-prop.}, \end{cases} \quad (9)$$

where  $L$  is the fiber length.

For the experimental SpRS noise measurements, only the pump wave was transmitted. The pump power at the fiber input was set to  $2.7 \text{ dBm}$  in the UC-MCF setup, and maintained at  $29 \text{ dBm}$  in the CC-MCF. All other experimental settings were identical to those used for the SRS gain measurements.

Figure 1(b) shows the SpRS efficiency for the UC-MCF, where solid lines represent SpRS efficiency derived from noise measurements, while dashed lines are the values estimated from the SRS gain efficiency using the analytical relation in Eq. (7), assuming a waveguide temperature of  $283 \text{ K}$ . Noise measurements are corrupted by the unfiltered laser's longitudinal modes. In order to remove the contribution of the unfiltered laser's modes and isolate the pump SpRS noise, we subtract a scaled version of the measured noise profile, adjusted for each mode launch power and attenuation. The SpRS efficiency extracted from noise measurements is in good agreement with the values obtained from the SRS gain estimates, with a divergence at the largest anti-Stokes shift due to the device noise floor of the OSA.

In Fig. 1(c), we plot the SpRS efficiency for the UC-MCF and CC-MCF. For the CC-MCF, the SpRS efficiency derived from SRS gain is identical for the co- and counter-propagating cases, as the Raman gain is independent of signal direction [4]. Curves from noise measurements, however, show small differences between both directions, although SpRS is theoretically direction-independent. Overall, the SpRS spectra for both fibers in all scenarios match in shape and are close in magnitude to those obtained from the SRS gain efficiency values.

As previously observed, in Fig. 1(c), the CC-MCF curves show a four-fold reduction in the group-averaged SpRS efficiency compared to the UC-MCF, due to the larger number of degenerate modes. Therefore, for the same pump power per

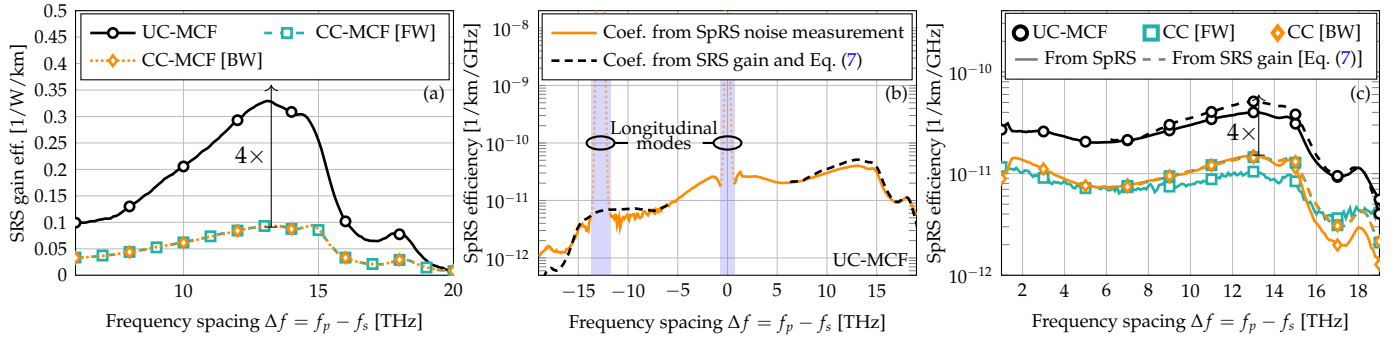


**Fig. 1.** (a) Mode-group-averaged SRS gain efficiency measured in the UC-MCF (solid line, circles), copropagating CC-MCF (dashed, squares), and counter-propagating CC-MCF (dotted, diamonds) configurations. Gain curves for the CC-MCF are extracted from [4]. (b) Estimated SpRS efficiency in the 4-core UC-MCF, obtained from copropagating noise (solid lines) and on-off gain (dashed lines) data, normalized by bandwidth. Shaded regions indicate the bandwidth of the unfiltered longitudinal laser modes. (c) Estimated SpRS efficiency from experimental measurements in the 4-core UC-MCF (circles) and 4-core CC-MCF (squares: copropagating, diamonds: counter-propagating), obtained from noise (solid lines) and on-off gain (dashed lines) data. The labels “FW” and “BW” represent, respectively, co- and counter-propagating measurements.

core, each core of the UC-MCF accumulates the same SpRS noise as in the CC-MCF.

The same characterization was performed on a 15-mode (5-mode-group) 50-km long graded-index MMF [16], deployed in the same testbed. The mode-group-averaged effective and cross-effective areas are shown in Fig. 2(a). Within conventional transmission bands, the self- and cross-effective mode areas have a negligible dependence on frequency, and are assumed as constant.

For the SpRS characterization, the pump was launched sequentially into each available mode, and the corresponding backscattered noise was measured with the OSA for each individual mode. The pump power launched into the mode-multiplexer was measured to be, on average, 19.70 dBm, with small variations across the selected pump configurations due to differing insertion losses among the optical paths. The crosstalk and mode-dependent losses of the multiplexer were derived from C-band measurements and presented in [17].

Linear mode coupling must be considered in MMFs measurements, as crosstalk is usually non-negligible. Coupling coefficients are measured for the pump frequency and for the signal band with a 1520-to-1580 nm noise source. The mode-group- and frequency-averaged values are given in Fig. 2(b). Minor frequency-dependent deviations were observed between coupling coefficients, therefore, the same coupling matrix was

considered for the pump and signal. Losses showed significant frequency-dependence, with the mode-group-averaged values plotted in Fig. 2(c), estimated from a polynomial interpolation of the experimentally measured values.

Supplementing Eq. (9) with terms accounting for linear coupling and inter-modal scattering, the material SpRS efficiency  $\hat{\eta}$  can be estimated from SpRS noise values measured in any arbitrary mode-group  $n$ , as given by

$$\hat{\eta}(f_p, \Delta f) = \begin{cases} \frac{P_{s,n}^{\text{SpRS}}(L)}{\left\{ \int_0^L e^{(\text{dg}(\alpha_s) - \mathbf{K}_s)(z'-L)} \mathbf{A}_{\text{eff}}^{\text{inv}} \bar{P}_p^{\text{T}}(z') dz' \right\}'_n}, & \text{Co-prop.,} \\ \frac{P_{s,n}^{\text{SpRS}}(0)}{\left\{ \int_0^L e^{-[\text{dg}(\alpha_s) + \mathbf{K}_s]z'} \mathbf{A}_{\text{eff}}^{\text{inv}} \bar{P}_p^{\text{T}}(z') dz' \right\}'_n}, & \text{Counter-prop.,} \end{cases} \quad (10)$$

where  $\mathbf{A}_{\text{eff}}^{\text{inv}}$  is a matrix whose elements are the mode-group-averaged inverse effective areas  $\tilde{A}_{\text{eff},i,h}^{-1}$ , the function  $\text{dg}(\cdot)$  denotes the matrix diagonal operator,  $\alpha_s$  and  $\mathbf{K}_s$  are for the signal frequency the attenuation vector and coupling matrix respectively, and  $\bar{P}_p^{\text{T}}(z)$  is the total pump power vector at distance  $z$ .

The measured mode-group-averaged backscattered SpRS noise, is shown in Fig. 3(a) for the pump launched in the 1<sup>st</sup> and 5<sup>th</sup> mode groups. We observe significant deviations in the noise levels when the pump was launched into the fundamental mode group, which are notably reduced when the pump was launched into the highest-order mode group. These deviations in noise levels are directly related to the overlap between mode groups, as indicated by the effective-area matrix shown in Fig. 2(a).

From Eq. (10), with the pump allocated in the fundamental mode-group, we obtain the SpRS efficiency curves shown in Fig. 3(b). Estimates derived from noise values across all mode groups are in excellent agreement, with minor deviations near the pump frequency.

In Fig. 3(c), we plot the mode-group-averaged measurements for each pump configuration. All measurements are in excellent agreement throughout the entire evaluated region, indicating that the SpRS efficiency can be reliably estimated using any pump configuration. Estimates derived from the SRS efficiency are not presented, as although Raman gain profiles were measured in the same fiber [7], measurements of the SRS coefficients in MMFs remain an ongoing effort, and no such characterization

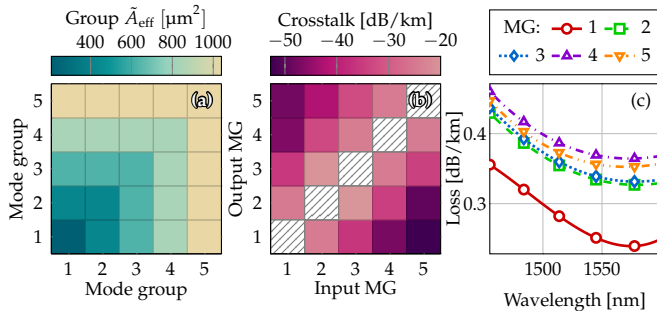


**Fig. 2.** (a) Self- and cross-effective areas of MMF mode-groups. (b) Mode-group-averaged coupling coefficients and (c) mode-group-averaged frequency-dependent attenuation of the MMF.

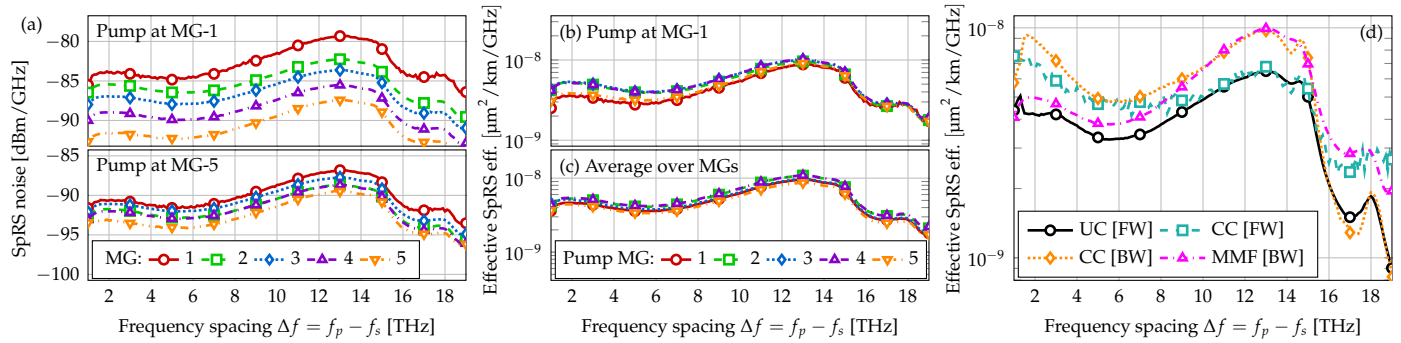


**Fig. 3.** (a) Per-mode counter-propagating SpRS noise in each mode group (distinguished by line styles) of the MMF, with the pump launched into the 1<sup>st</sup> and 5<sup>th</sup> mode groups. (b) Effective SpRS efficiency estimated from measurements of each mode group with the pump in the fundamental mode. (c) Mode-group-averaged measurements for each pump configuration. (d) Effective SpRS efficiency for the different SDM fiber types, where the MMF curve correspond to the average over all measurements.

has yet been reported.

As the material SpRS efficiency is independent of fiber design, it can be directly compared across different fiber types. Figure 3(d) shows the material SpRS efficiency extracted from noise measurements for the UC-MCF, CC-MCF, and MMF. The efficiencies lie within a similar range, showing close agreement between all fiber designs, with the co-propagating UC-MCF estimation marginally lower. While small deviations are expected due to variations in doping concentrations among different fiber designs, direction-dependent discrepancies may arise from backscattering at splices or span connections. Overall, the agreement observed across distinct fiber types indicates that a mode-independent SpRS profile can be extracted irrespective of the fiber design, with the mode profiles accounted for solely through the effective-area matrix.

To conclude, we develop a generalized model for the longitudinal evolution of SpRS power in SDM fibers with multiple mode groups, extending prior formulations for SMFs by decomposing the SpRS efficiency as the product of a material-dependent term and a dimensional overlap factor between the interacting modes. Additionally, the model relates the SpRS coefficient in both the Stokes and anti-Stokes regions to the SRS efficiency. The model is utilized to characterize the SpRS efficiency experimentally in three field-deployed SDM fibers, a 4-core UC-MCF, a 4-core CC-MCF, and a 15-mode graded-index MMF. Measurements show good agreement between analytical estimates derived from previously reported SRS efficiency data and SpRS efficiency derived from the received scattered noise, as well as consistent across the considered fibers. These results advance the understanding of non-linear impairments in SDM links where SpRS is non-negligible, a regime that is particularly relevant for the coexistence of classical optical communication and QKD.

**Funding.** Funded by the European Union (Grant Agreement 101120422 and 101072409). Views and opinions expressed are, however, those of the author(s) only and do not necessarily reflect those of the European Union or REA. Neither the European Union nor the granting authority can be held responsible for them.

**Disclosures.** The authors declare no conflicts of interest.

**Data availability.** Data underlying the results presented in this paper are not publicly available at this time but may be obtained from the authors upon reasonable request.

## REFERENCES

1. P. J. Winzer, *IEEE Photonics J.* **4**, 647 (2012).
2. T. A. Eriksson, B. J. Puttnam, G. Rademacher, *et al.*, "Inter-core crosstalk impact of classical channels on CV-QKD in multicore fiber transmission," in *Optical Fiber Communications Conference and Exhibition (OFC)*, (Optica, 2019), pp. 1–3.
3. R. Kumar, H. Qin, and R. Alléaume, *New J. Phys.* **17**, 043027 (2015).
4. G. Di Sciullo, L. A. Zischler, D. A. Shaji, *et al.*, *J. Light. Technol.* **44**, 79 (2026).
5. J. Schneck, L. A. Zischler, B. Kalla, *et al.*, "Experimental Characterization of Mode-Dependent Stimulated Raman Scattering in a 15-Mode Fiber," in *51th European Conference on Optical Communications (ECOC)*, (2025), pp. 1–4.
6. L. A. Zischler, J. Schneck, G. Di Sciullo, *et al.*, "Evaluation of Inter-Mode-Group Stimulated Raman Scattering on Multi-Mode Fibers," in *2025 IEEE Photonics Conference (IPC)*, (IEEE, 2025), pp. 1–2.
7. D. A. Shaji, J. Schneck, L. A. Zischler, *et al.*, "Raman Gain Profiling and Distributed Raman Amplification in a Field-Deployed 15-Mode Graded-Index Multimode Fiber," in *Optical Fiber Communications Conference and Exhibition (OFC)*, (Optica, 2026).
8. K. Rottwitz, J. Bromage, A. J. Stentz, *et al.*, *J. Light. Technol.* **21**, 1652 (2003).
9. J. Bromage, *J. Light. Technol.* **22**, 79 (2004).
10. C. Antonelli, A. Mecozzi, A. Marotta, *et al.*, "Space-Division Multiplexed Transmission in Deployed Fibers," in *2025 30th OptoElectronics and Communications Conference (OECC) and 2025 International Conference on Photonics in Switching and Computing (PSC)*, (IEEE, 2025), pp. 1–4.
11. Q. Lin, F. Yaman, and G. P. Agrawal, *Phys. Rev. A-Atomic, Mol. Opt. Phys.* **75**, 023803 (2007).
12. C. Antonelli, A. Mecozzi, and M. Shttaif, *Opt. letters* **38**, 1188 (2013).
13. R. Hellwarth, J. Cherlow, and T.-T. Yang, *Phys. Rev. B* **11**, 964 (1975).
14. F. Poletti and P. Horak, *J. Opt. Soc. Am. B* **25**, 1645 (2008).
15. T. Hayashi, T. Nagashima, T. Nakanishi, *et al.*, "Field-deployed multi-core fiber testbed," in *2019 24th OptoElectronics and Communications Conference (OECC) and 2019 International Conference on Photonics in Switching and Computing (PSC)*, (IEEE, 2019), pp. 1–3.
16. P. Sillard, D. Molin, M. Bigot-Astruc, *et al.*, *J. Light. Technol.* **34**, 425 (2016).
17. A. Gatto, P. Parolari, R. S. Luis, *et al.*, *J. Light. Technol.* **42**, 4720 (2024).

## FULL REFERENCES

1. P. J. Winzer, "Optical networking beyond WDM," *IEEE Photonics J.* **4**, 647–651 (2012).
2. T. A. Eriksson, B. J. Puttnam, G. Rademacher, *et al.*, "Inter-core crosstalk impact of classical channels on CV-QKD in multicore fiber transmission," in *Optical Fiber Communications Conference and Exhibition (OFC)*, (Optica, 2019), pp. 1–3.
3. R. Kumar, H. Qin, and R. Alléaume, "Coexistence of continuous variable QKD with intense DWDM classical channels," *New J. Phys.* **17**, 043027 (2015).
4. G. Di Sciullo, L. A. Zischler, D. A. Shaji, *et al.*, "Characterization of Stimulated Raman Scattering in Field-Deployed Coupled-Core Multi-Core Fibers," *J. Light. Technol.* **44**, 79 (2026).
5. J. Schneck, L. A. Zischler, B. Kalla, *et al.*, "Experimental Characterization of Mode-Dependent Stimulated Raman Scattering in a 15-Mode Fiber," in *51th European Conference on Optical Communications (ECOC)*, (2025), pp. 1–4.
6. L. A. Zischler, J. Schneck, G. Di Sciullo, *et al.*, "Evaluation of Inter-Mode-Group Stimulated Raman Scattering on Multi-Mode Fibers," in *2025 IEEE Photonics Conference (IPC)*, (IEEE, 2025), pp. 1–2.
7. D. A. Shaji, J. Schneck, L. A. Zischler, *et al.*, "Raman Gain Profiling and Distributed Raman Amplification in a Field-Deployed 15-Mode Graded-Index Multimode Fiber," in *Optical Fiber Communications Conference and Exhibition (OFC)*, (Optica, 2026).
8. K. Rottwitt, J. Bromage, A. J. Stentz, *et al.*, "Scaling of the Raman gain coefficient: applications to germanosilicate fibers," *J. Light. Technol.* **21**, 1652–1662 (2003).
9. J. Bromage, "Raman amplification for fiber communications systems," *J. Light. Technol.* **22**, 79 (2004).
10. C. Antonelli, A. Mecozzi, A. Marotta, *et al.*, "Space-Division Multiplexed Transmission in Deployed Fibers," in *2025 30th OptoElectronics and Communications Conference (OECC) and 2025 International Conference on Photonics in Switching and Computing (PSC)*, (IEEE, 2025), pp. 1–4.
11. Q. Lin, F. Yaman, and G. P. Agrawal, "Photon-pair generation in optical fibers through four-wave mixing. Role of Raman scattering and pump polarization," *Phys. Rev. A-Atomic, Mol. Opt. Phys.* **75**, 023803 (2007).
12. C. Antonelli, A. Mecozzi, and M. Shtaif, "Raman amplification in multi-mode fibers with random mode coupling," *Opt. letters* **38**, 1188–1190 (2013).
13. R. Hellwarth, J. Cherlow, and T.-T. Yang, "Origin and frequency dependence of nonlinear optical susceptibilities of glasses," *Phys. Rev. B* **11**, 964 (1975).
14. F. Poletti and P. Horak, "Description of ultrashort pulse propagation in multimode optical fibers," *J. Opt. Soc. Am. B* **25**, 1645–1654 (2008).
15. T. Hayashi, T. Nagashima, T. Nakanishi, *et al.*, "Field-deployed multi-core fiber testbed," in *2019 24th OptoElectronics and Communications Conference (OECC) and 2019 International Conference on Photonics in Switching and Computing (PSC)*, (IEEE, 2019), pp. 1–3.
16. P. Sillard, D. Molin, M. Bigot-Astruc, *et al.*, "Low-differential-mode-group-delay 9-LP-mode fiber," *J. Light. Technol.* **34**, 425–430 (2016).
17. A. Gatto, P. Parolari, R. S. Luis, *et al.*, "Partial-MIMO based mode-group transmission and routing in a field-deployed 15-mode network: throughput, DSP resources and network flexibility," *J. Light. Technol.* **42**, 4720–4732 (2024).